From tensor-product to truncated hierarchical B-splines: Enhancing spatial resolution in space-continuous deformation analysis based on 3D point clouds

Elisabeth Ötsch[1], Hans Neuner[1]

[1]TU Wien, Department of Geodesy and Geoinformation, Wiedner Hauptstraße 8-10, 1040 Vienna, Austria
elisabeth.oetsch@tuwien.ac.at, hans.neuner@geo.tuwien.ac.at

Keywords: deformation analysis, surface representation, local refinement, tensor-product B-splines, truncated hierarchical B-splines

Abstract

The quasi-continuous capturing of our environment by terrestrial laser scanning (TLS) in form of 3D point clouds provides the basis for numerous spatial analyses, including space-continuous deformation analysis. In times of aging infrastructure and climate change-induced, cumulative mass movements, statistically-sound methods for determining areal deformations are becoming increasingly important. However, the lack of reproducibility of absolute point positions between consecutive scans and the presence of measurement noise demand approaches that retrieve credible comparison statements. The representation of point clouds by geometric surfaces supports noise reduction and serves as basis for successive analysis. Tensor-product B-spline surfaces have proven to be particularly versatile geometric representations to derive spatially consistent deformation estimates. This paper extends this concept by investigating the use of truncated hierarchical B-splines for statistically sound deformation analysis. We show that deformation is detectable when partition of unity is preserved through truncation. In a simulated environment, significant deformations between two point clouds were successfully detected. Results indicate that coarse surface representations lead to type-1 errors and underestimated deformation magnitudes, whereas more refined surface representations yield consistent deformation estimates, providing a potential termination criterion for adaptive model refinement.

1. Introduction

In times of aging infrastructure and climate change-induced, cumulative mass movements, *statistically sound* methods for determining areal deformations are becoming increasingly important. The use of LiDAR techniques for fast and rigorous data acquisition at high accuracy levels may serve as basis for those analyses. The landscape of developed methodologies for proper point cloud comparisons is manifold, as different scenes demand different approaches to derive information about spatial resp. temporal stability. An overview and systematizations of established procedures are compiled in Qin et al. (2016) or Mukupa et al. (2017).
The category of surface-to-surface based approaches for point cloud comparisons is beneficial for the sake of statistically sound deformation analysis as it tackles two key challenges. First, the approximation of point clouds by geometrical surfaces as optimization problem allows the inclusion of stochastic information of the scanned data. This enables subsequent application of rigorous test statistics of estimated surface parameters forming the deformation analysis. Second, point cloud approximation by surfaces filters the random noise to a large extent, thus enabling the detection of deformations even in cases when these exceed the measurement noise by only a small extent.
In many research projects accomplished up to now, the suitability of B-splines for the representation of curves or surfaces from TLS-point clouds and the subsequent statistical rigorous deformation analysis was investigated and proven (Bureick, 2020; Harmening, 2020; Kerekes, 2023; Raschhofer et al., 2021). All these approaches employ a global representation of surfaces by tensor-product B-splines (TP B-splines). This means, that the B-spline basis functions and their corresponding knots are active over the entire surface. Cases, where the surface exhibits local geometric characteristics or presents localized deformations, can still be captured by adding additional basis functions (and corresponding knots) to the TP B-spline surface representation. However, this leads in consequence to an increased complexity of the representation models as the number of control points that need to be estimated increases. As the corresponding functions are active over the entire surface, this leads to an over-parameterization in areas where the surface representation is smoother and can be estimated sufficiently well by the initial parameterization.

To prevent rapid increase in complexity different local refinement strategies were developed. Their common concept is to introduce additional basis functions in the course of a refinement stage, but to activate them only in the necessary parts of the surface. In this way, the number of parameters to be estimated is limited to the necessary extent. Some of the developed strategies are hierarchical B-splines (Forsey and Bartels, 1989), truncated hierarchical B-splines (Giannelli et al., 2012), LR B-splines (Dokken et al., 2013, 2015; Skytt et al., 2015) or T-splines (Sederberg et al., 2003).

First steps in adapting local refinement strategies for geodetic problems restricted to curve and surface approximation are presented in Kermarrec et al. (2020) concerning hierarchical B-splines as well as in Kermarrec et al. (2022b) concerning the application of LR B-splines for monitoring of coastal areas. Mohammadivojdan et al. (2025) employed hierarchical B-splines to detect and remove outliers from bathymetric data recorded by multibeam echosounder systems. A comprehensive insight into representing terrain and seabed data by LR B-splines is provided by Kermarrec et al. (2022a).

None of these approaches have been yet employed for a comprehensive deformation analysis based on rigorous test statistics on surface parameters. Thus, the main novelty of this paper

This contribution has been peer-reviewed. The double-blind peer-review was conducted on the basis of the full paper.
https://doi.org/10.5194/isprs-annals-XI-1-2026-401-2026

lies in the investigation of the local refinement for deformation analysis purposes. Herefore, we focus on the enhancement of global (TP) B-splines to truncated hierarchical B-splines (THBS). The key aspects addressed in this contribution are as follows:

1. Assessment of the applicability of the deformation analysis to estimated control points based on THBS across different levels of refinement
2. Investigation of the role of truncation in preserving the partition of unity, which is essential for adequate parameter estimation
3. Evaluation within a simulation environment to analyse the identified mangitude and regional spread of the detected deformation under nominal conditions

This study is conducted in the framework of the TLS-Defo project. In this project, the research unit adopts a holistic approach to develop a statistical rigorous method for TLS-based deformation analysis. To achieve this goal, several challenges comprising the surface representation, the calibration of terrestrial laser scanners, the quantification of measurement uncertainty as well as of the model uncertainty are tackled in distinct but coordinated research projects. This work is part of the project called ”Surface representation and deformation analysis” dealing with the estimation of displacement vectors and with conducting the deformation analysis tests.

The remainder of this paper is structured as follows: The 2^{nd} Section introduces the methodological basis. The 3^{rd} Section contains the setup of the simulation environment. The obtained results and their discussion form the content of Sections 4 and 5 respectively. A section with conclusions and an outlook on future work ends the paper.

2. Methodology

2.1 Deformation analysis based on approximating B-spline surfaces

The most general form of B-spline surfaces being the tensor-product B-spline surface is mathematically defined by

$$\mathbf{S}(u,v) = \sum_{i=0}^{m}\sum_{j=0}^{n} N_{i,p}(u)N_{j,q}(v)\cdot \mathbf{P}_{i,j}. \tag{1}$$

A surface point $\mathbf{S}(u,v)$ is described as the weighted compound of corresponding control points $\mathbf{P}_{i,j}$. The weights $N_{i,p}(u)$ resp. $N_{j,q}(v)$ are B-spline basis functions, recursively constituted via the Cox-de-Boor formula (Cox, 1972). The local impact of one control point $\mathbf{P}_{i,j}$ on the surface is related to the knot spacing in the knot vectors $\mathbf{U} = [u_i, ..., u_{m+p+1}]$ resp. $\mathbf{V} = [v_j, ..., v_{n+q+1}]$ and the B-splines degree p resp. q. For more details, we refer to Piegl and Tiller (2012).

In the context of space-continuous deformation analysis, B-spline surfaces showcase particular suitability as the B-spline basis functions $N_{i,p}(u)$ resp. $N_{j,q}(v)$ exhibit local support over consecutive regions of the surface. Consequently, local surface deformation can be mathematically represented as displacement of corresponding control points. This characteristic enables the introduction of the estimated control points into the well-established congruency model (Eichhorn et al., 2013, p. 488ff) to detect and identify statistically sound deformation between two sets of control points (Ötsch et al., 2023). Thus, the space-continuous deformation analysis can be reformulated as a point-wise analysis without compromising the ability to interpret areal deformation behaviour.

The congruence of the B-spline surfaces estimated from point clouds in two epochs can be formulated as null hypothesis regarding the displacement between control points:

$$H_0 : E[\mathbf{d}_{i,j}] = E[\mathbf{P}^{(2)}_{i,j} - \mathbf{P}^{(1)}_{i,j}] = \mathbf{0} \tag{2}$$

Herein, the vector $\mathbf{d}$ represents the coordinate difference of corresponding control points in the two epochs (2) and (1). A possible rejection of the null hypothesis with the type 1 error α is tested statistically employing the test statistic (Pelzer, 1985, p. 586):

$$F = \frac{\mathbf{d}^T {\mathbf{Q}_{\mathbf{dd}}}^{-1}\mathbf{d}}{\hat{\sigma}_0^2 \cdot h} \sim F_{h,(r_1+r_2)}, \tag{3}$$

where $\mathbf{Q_{dd}}$ is the cofactor matrix of the differences between control points, h corresponds to the rank of $\mathbf{Q_{dd}}$ and $\hat{\sigma}_0^2$ is the aggregated variance of the unit weight of the adjustments of the two epochs. In the case that the null hypothesis holds, F follows a Fisher distribution with h and $(r_1 + r_2)$ degrees of freedom, where r_1 and r_2 is the redundancy of the adjustment in the epochs (1) and (2) respectively. The test result indicates the presence of deformations (rejection of the null hypothesis) if:

$$\hat{F} > F_{h,(r_1+r_2),1-\alpha}, \tag{4}$$

where $F_{h,(r_1+r_2),1-\alpha}$ is the quantile of the corresponding Fisher-distribution. In that case, a subsequent step localizes the significantly displaced control points. In this study, the localization according to the decomposition of disclosures according to Gauss is used (Pelzer, 1985, p. 592ff). The idea of this method is to iteratively assume that each control point $\mathbf{P_{i,j}}$ is displaced and calculate the specific measure:

$$\mathbf{R_{d,i,j}} = \overline{\mathbf{d}}^T_{d,i,j} \cdot \mathbf{P_{dd,i,j}} \cdot \overline{\mathbf{d}}_{d,i,j}, \tag{5}$$

where $\overline{\mathbf{d}}_{d,i,j}$ is the coordinate difference between the locations of the suspected control point $\mathbf{P_{i,j}}$ in the two epochs, de-correlated from the other coordinate differences of the control points, and P_{dd} is its corresponding weight matrix.The control point that leads to the highest value of all $\mathbf{R_d}$ is localised as significantly displaced.

2.2 Transition from TP B-splines to hierarchical B-splines in the context of deformation analysis

The representation of point clouds by TP B-splines is suitable for consecutive deformation analysis as long as the scanned surface is smooth. As the control points are linked to a regular knot-grid (see Figure 3(a)), refinement is always accompanied by addition of an extra line or column of knots throughout the whole surface. Hence, extensive refinement of a TP B-spline surface is leading to rapidly increasing computational costs. Here approaches of locally refineable B-splines come into play.

In this context local refinement denotes the increase of surface resolution in locally distinct regions. This is accompanied by

insertion of local patches of superior resolution in the knot-grid (see Figure 3(b) and 3(c)), which enables high-resolution surface representation at desired regions whilst keeping parameter sparsity elsewhere.

Among various locally refineable B-spline formulations, hierarchical B-spline surfaces (HBS) constitute adaptive surface representations. They are obtained by a multilevel refinement scheme, where successively levels of detail ℓ are introduced to generate a nested B-spline space defined on a domain $\Omega = \Omega^0 \subset \Omega^1 \subset \cdots \subset \Omega^L = \emptyset$ (Garau and Vázquez, 2018). The respective levels are separable TP B-spline surfaces with different resolutions. The knot vectors $\mathbf{U}^\ell$ resp. $\mathbf{V}^\ell$ with $\ell = 1, \ldots, L$ align with the nested nature of the spaces such as the knots within the knot vectors $\mathbf{U}^\ell$ resp. $\mathbf{V}^\ell$ are also part of $\mathbf{U}^{\ell+1}$ resp. $\mathbf{V}^{\ell+1}$. The consecutive degree of refinement can be chosen. In this paper we use dyadic knot refinement. Herein, each knot span is halved in one refinement step ℓ. The respective contribution of each nested level ℓ to the surface description is commonly stored in a mesh structure $\mathcal{G}^\ell$, that represents the knot-grid of the surface. It defines the active contributions of the subdomains Ω^ℓ to the compound of the surface description (see Figure 3). A hierarchical B-spline surface is mathematically defined as

$$\mathbf{S}(u,v) = \sum_{\ell=0}^{L} \left(\sum_{i \in \mathcal{A}^\ell} \sum_{j \in \mathcal{A}^\ell} N_{i,p}^\ell(u) N_{j,q}^\ell(v) \cdot \mathbf{P}_{i,j}^\ell \right), \qquad (6)$$

whereas $\mathcal{A}^\ell$ is the compound of active basis functions on each level. A more elaborate description of the mathematical defintion of HBS can be found in Forsey and Bartels (1989) and Garau and Vázquez (2018).

2.3 Truncation

The basis functions of a TP B-spline surface, by definition, always sum up to one, forming partition of unity. When combining several levels of successively refined B-spline surfaces to form an HBS surface, this characteristic is violated due to the overlap between active basis functions on level $\ell - 1$ and ℓ. This aspect also affects the estimability of unknown control points in a GMM as redundant support of basis functions from different levels impact among others the condition number of the normal matrix (Giannelli et al., 2012). Truncation of the basis functions of inferior levels is used to maintain partition of unity of the basis functions over the nested B-spline space. This procedure is profoundly examined in Giannelli et al. (2012) and shall be briefly addressed in the following:
The principle of truncation builds upon the fact, that each basis function on a coarser level $\ell - 1$ can be represented as a linear combination of basis functions of the refined level ℓ. The respective relationship depends on the degree of the B-spline surface and the refinement scheme (e.g., dyadic knot refinement). An example for the truncation of basis functions in parameter direction u is visualized in the Figures 1 and 2, showing the basis functions of a B-spline curve of degree $p = 2$.

In Figure 1 the basis functions of 2 levels $\ell = 0$ and $\ell = 1$ are visualized. The bold lines indicate the basis functions, that are active on each level, i.e. $N_i^\ell \in \mathcal{A}^\ell$. In Figure 2 the combined basis functions are illustrated: Figure 2(a) shows the basis functions for HBS, consisting of stacking active basis functions over both levels. The basis function N_3^0 is replaced by the basis

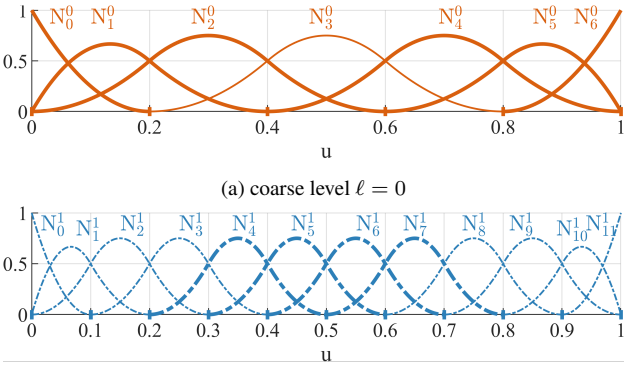

(a) coarse level $\ell = 0$

(b) refined level $\ell = 1$

Figure 1. Basis functions of two B-spline levels of degree $n = 2$

functions N_{4-7}^1. Figure 2(b) shows the stacked basis functions, where the coarser level is truncated for the sake of maintaining partition of unity. The basis function N_3^0 is substituted by the functions N_{4-7}^1, likewise as above. At the same time neighbouring basis functions, whose support overlap with active basis functions from refinement level $\ell = 1$ are modified. For the mathematical definition of the truncation procedure we refer to Giannelli et al. (2016) and Hennig et al. (2016).

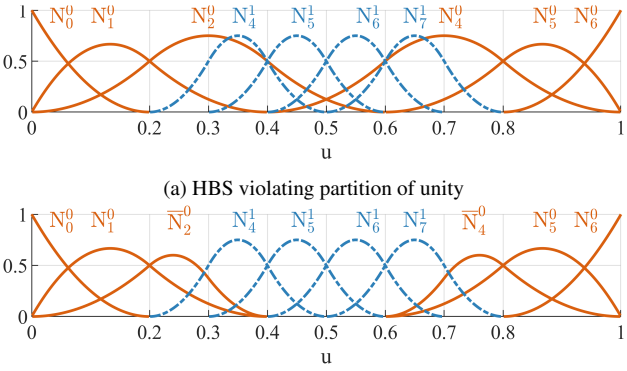

(a) HBS violating partition of unity

(b) THBS warranting partition of unity

Figure 2. Stacked B-spline basis functions

To outline the impact of truncation the following example is given: The basis function N_2^0 can be expressed as the linear combination:

$$N_2^0 = \frac{1}{4}N_2^1 + \frac{3}{4}N_3^1 + \frac{3}{4}N_4^1 + \frac{1}{4}N_5^1. \qquad (7)$$

The basis functions N_4^1 and N_5^1 are active in $\mathcal{A}^1$ and thus, in the course of truncation their contribution to the linear combination is eliminated resulting in

$$\overline{N}_2^0 = \frac{1}{4}N_2^1 + \frac{3}{4}N_3^1. \qquad (8)$$

The truncation for N_4^0 is performed equally. D’Angella et al. (2018) propose the generation of a transition matrix combining the coefficients of the linear combinations for the simultaneous truncation of multiple basis functions.

At this point, it is important to consider how truncation is affected when open knot vectors are used, i.e., when the outer

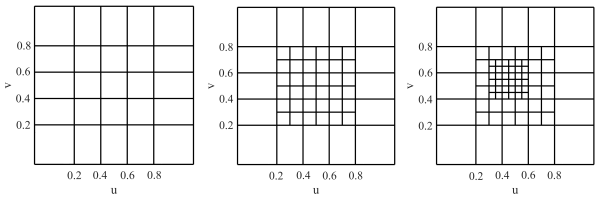

(a) L = 0 (b) **L = 1** (c) L = 2

Figure 3. Knot-grids illustrating the stacked refinement levels ℓ for all investigated surface representations

knots have multiplicity $p + 1$ resp. $q + 1$. Open knot vectors are commonly employed in surface fitting, since they enforce interpolation at the boundaries of the surface (Piegl and Tiller, 2012). Because the exterior basis functions differ in shape and support from the interior basis functions (compare $N_0^0, N_1^0, N_5^0, N_6^0$ in Figure 1(a)), the linear combinations used in the standard truncation procedure must be adjusted near the boundaries. In these regions, the hierarchical refinement involves fewer overlapping basis functions from higher levels, leading to modified truncation weights in the resulting linear combinations. For further details, we refer to Kiss et al. (2014) and Giannelli et al. (2016).

3. Experiments

3.1 Establishment of a simulation environment

Since, to the best of our knowledge, this is the first investigation of local refinement strategies for the purpose of deformation analysis from point clouds, it is initially based on simulated data. This enables to examine the performance and limitations of this strategy without the results and the drawn conclusions being biased by other influences from the measurement process and the unforeseen behavior of the object. We are aware that there exist powerful tools for the establishment of near real simulation environment of laser scanning data (e.g., HELIOS++, Winiwarter et al. (2022)). Though, we decided on using a nominal B-spline surface as basis for the simulation setup. Herethrough, we can focus on the sole aspect of local refinement in the course of deformation analysis and minimize superposition of effects retrieved from the (assumed) scanning geometry. Nevertheless, the dimensions and units reflect representative measures of a conventional laser scanning scenario for the sake of better interpretability.

The starting point for the simulation is a TP B-spline surface that is based on 7×7 control points and second-degree B-spline functions. The corresponding knots are distributed evenly in the normalised range [0, 1]. In the central area of the surface in the range of surface parameters [0.2 – 0.8] × [0.2 - 0.8], a first refinement level of the surface is incorporated using the method described in section 2. In each parameter direction, an additional knot is introduced in the center of each of the three knot spans. The resulting mesh of the parameter lines is shown in Figure 3(b). This surface represents the nominal surface of the first epoch. The linkage between the knot-grid, the THBS surface and the control points is schematically visualized in Figure 4(a).

The nominal surface of the second epoch is obtained by shifting a selected control point of the first refinement level along the z-axis. This is illustrated in Figure 4(b). Three scenarios are considered: (i) no displacement, (ii) a displacement of 10mm,

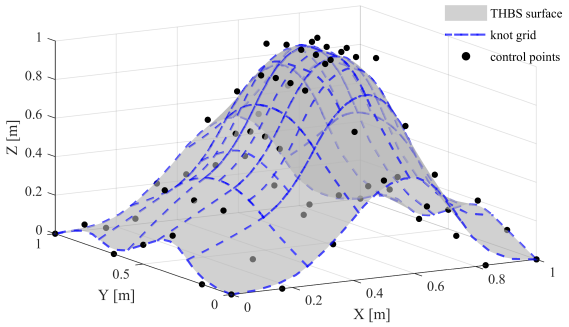

(a) Nominal THBS surface with control points and knot grid forming the reference epoch

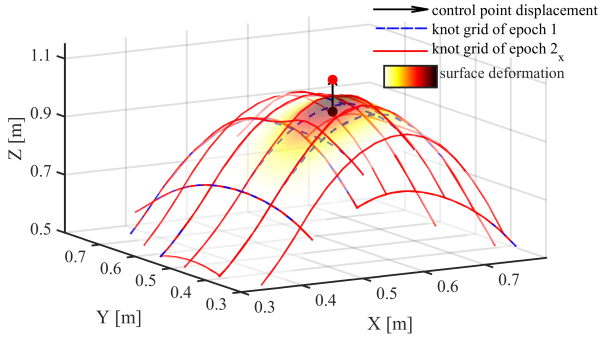

(b) Generation of the nominal THBS surface by displacement of one control point causing local displacement of the surface. Magnitude scaled for better visualisation.

Figure 4. schematic examples of the established nominal surfaces

and (iii) a displacement of 20mm. The first scenario corresponds to the null hypothesis stated in Equation 2, whereas the latter two represent cases in which the null hypothesis is violated. A displacement of 20mm at the control point results in a maximum surface displacement of approximately 11.2mm, while a 10mm shift leads to a maximum surface displacement of 5.6mm. To distinguish between the scenarios, the corresponding surface and the points sampled on it in the second epoch are referenced by epoch 2_0, 2_{20} and epoch 2_{10}.

The chosen displacement magnitudes ensure that (i) a clearly detectable deformation is present and (ii) the resulting maximum surface displacement remains on the order of the noise level (see below). This setup enables the investigation of how localized control point displacements influence the B-spline-based deformation analysis at different refinement stages, particularly with respect to the estimated magnitude and spatial extent of deformation.

For both epochs, the nominal surfaces are discretised into 4900 points by sampling on a regular grid. Synthetic observations are generated by superimposing white noise with a standard deviation of 2mm in each coordinate direction. In the 2_{10} scenario, the resulting surface differences are in the order of three times the noise standard deviation in the z-direction, representing a near-detection-limit (marginal) case.

The point clouds obtained in this way were then fed into the deformation analysis using THBS surfaces. To ensure the representativeness of the results, 1000 simulation runs were performed, with the noise being regenerated in each run.

3.2 Pipeline of data analysis

The space-continuous deformation analysis is based on statistical evidence of the displacement of control points of the B-spline surfaces that approximate the point clouds generated above. Three different refinement levels were employed to represent the respective surfaces from point clouds. The Level 0 (L = 0) representation corresponds to the classic TP B-spline representation (see knot-grid in Figure 3(a)). The Level 1 (L = 1) representation reflects the nominal refinement level of the surface representation and thus represent the ground truth (see knot-grid in Figure 3(b)). With the introduction of a further refinement level, the Level 2 (L = 2) representation, the effect of excessive refinement on the deformation analysis is investigated (see knot-grid in Figure 3(c)). The region targeted for refinement was selected manually as automatic detection of regions requiring refinement lies beyond the scope of the present study. Interested readers are referred to Ötsch and Neuner (2025), where suitable indicators for the identification of refinement needs are investigated.

The number of control points in the Level 0 representation was selected using the Bayesian Information Criterion (BIC) as model selection criterion (Schwarz, 1978). The criterion was evaluated in a range from 5×5 to 15×15 control points in all possible combinations and reached its minimum for the nominal number of 7×7 control points. For the Level 1 and Level 2 representations, one control point of the lower resolution level was replaced by a new network of control points. The knot spans of the corresponding base function were halved.This resulted in a single control point being replaced by a 4×4 grid of new control points at the next refinement level. This transition occurs by substituting one tensor-product basis function at level L = 0 with a weighted sum of refined basis functions extending the 1D procedure stated in Equation (7). The Level 1 representation thus contains 48 + 16 = 64 control points and the Level 2 representation contains 48 + 15 + 16 = 79 control points.

The position of these control points was estimated in each simulation run for each epoch (1, 2_0, 2_{10} and 2_{20}). Subsequently, the stability of the control points was evaluated using the global congruency test (see Equation (2) - (4)) and displaced control points were localised employing Equation (5).

In Figure 5, the pipeline from the setup of the simulation study to the repetitive realisations of the surface approximation and subsequent deformation analysis is depicted.

4. Results

The results section is arranged in accordance to the simulation studies comprising four surface representations with three different levels of refinement for the three epoch comparisons. Each result comprises a quantitative analysis of the test statistics for all conducted simulation runs presented in table form and one representative example with the most frequent outcome retrieved in the 1000 repetitions presented as visualisation. Each result is analysed by describing the deformation magnitudes and their associated precision. In addition, the frequency class of outcomes converging to the most common result is examined through their first and second statistical moments. The visual display of the deformation results are restricted to the epoch comparison epoch 1 vs. epoch 2_{10}.

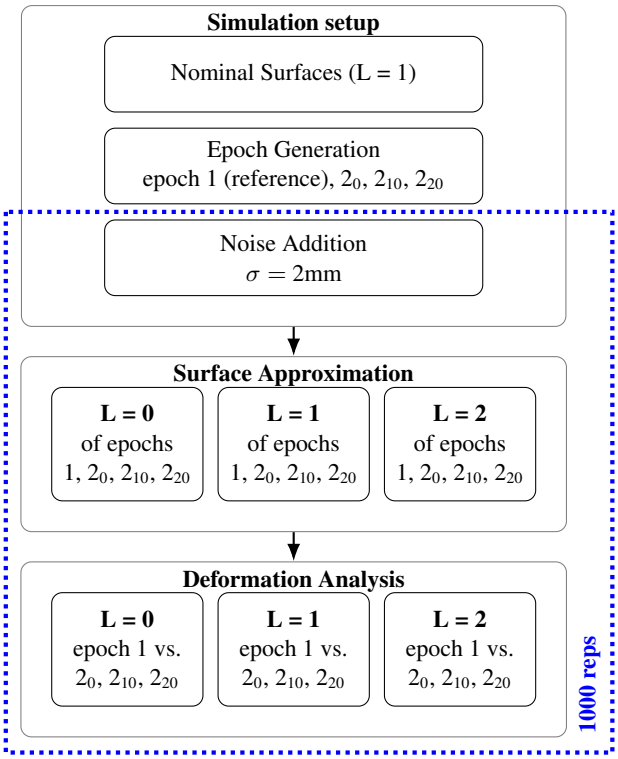

Figure 5. Pipeline of simulation study

4.1 Deformation analysis based on nominal surface representations

When using the nominal surface as model for point cloud approximation and subsequent deformation analysis, the null hypothesis is accepted for the epoch comparison epoch 1 vs. epoch 2_0. This outcome holds true for 95.1% of the realisations within the simulation runs. For the epoch comparisons epoch 1 vs. epoch 2_{20} and epoch 1 vs. epoch 2_{10} the null hypothesis of the congruency model is rejected. In both of these cases, the most frequent number of identified significantly deformed control points is one. This applies to 95.0% of the simulation runs for the epoch comparison epoch 1 vs. epoch 2_{10} and to 94.4% of the realisations for epoch comparison epoch 1 vs. epoch 2_{20}. The identified point aligns with the one modified to generate the deformation of the nominal control epochs. Table 1 summarizes the congruency test results and localization performance across all 1000 simulation runs.

ep.	**Congruency Test**		**Localization**
1 vs.	mean($\hat{\text{F}}$) (σ)	F($\alpha = 5\%$)	mode(sig. CP)
$\mathbf{2_0}$	1.002 (0.105)		0 of 64
$\mathbf{2_{10}}$	1.934 (0.176)	1.174	1 of 64
$\mathbf{2_{20}}$	4.766 (0.301)		1 of 64

Table 1. Comparison of results of the congruency test and localisation for the epoch comparisons based on surface representation L = 1 over all simulation runs

In Figure 6, a representative result of the epoch comparison epoch 1 vs. epoch 2_{10} is depicted. Among the stable control points, indicated as white dots, the control point identified as significantly displaced is marked black. Here, the determined interepochal Euclidean distance of this control point

is 9.7mm with a standard deviation of 1.1mm. The discrepancy of 0.3mm (3%) to the nominal displacement is thus not significant. The related maximum Euclidean distance between the compared surfaces is 5.3mm ($\sigma = 0.5$mm), corresponding to a 5% deviation from the nominal surface difference of 5.6mm.
Among all simulation runs yielding the same - most frequent - number and identification of significant control points, the mean magnitude of interepochal control point differences is 10.1mm (1% deviation from nominal), with an overall repeatability precision of 1.1mm. The mean surface difference over all realisations resolving to the same significance statement is 5.7mm (3% deviation from nominal) with a precision of 0.5mm. Concerning the region of identified deformation, the impact of the identified significant control point on the surface is marked by the black isoline. This can be directly derived from the weights of the control points.

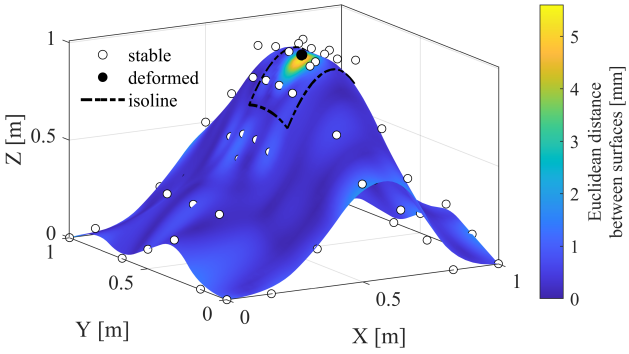

Figure 6. Representative result of the deformation analysis between epoch 1 and epoch 2_{10} based on surface representation L = 1

4.2 Deformation analysis based on surface representations of a lower refinement level

The approximation of the simulated data using a B-spline model of inferior model complexity is realised by removing the refinement layer of the nominal surface representation. Thereby, a TP B-spline surface with 7×7 control points is used. This model is confirmed using BIC, as stated in Section 3. Although this geometric model is less complex than the nominal one used for data generation, the global test of surface adjustment converges for the epochs 1 and 2_0 once the predefined variance–covariance matrix is applied. This result is expected, since the geometric course of this less complex surface representation aligns with the nominal surface. The situation differs for the comparison epochs 2_{10} and 2_{20}, where one control point is modified to introduce local deformation. As a result, the surface no longer follows the original, unrefined geometry.
Consequently, the approximation of these datasets with the TP B-spline surface of inferior complexity does not converge directly when the predefined variance–covariance matrix is applied. Insufficiencies of the functional model lead to the rejection of the null hypothesis in the global test of adjustment. To encounter that, the stochastic model was modified carefully by downweighting points according to their standardized residuals (Niemeier, 2008, p. 291ff).

The results of the deformation analysis based on the estimated control points over all simulation runs are stated in Table 2. In the case of the epoch comparison epoch 1 vs. epoch 2_0, the null hypothesis applies in 95.1% of the cases. For the other epoch comparisons significant deformation is detected within the set of control points. For the epoch comparison epoch 1 vs. epoch 2_{20}, the most frequent number of identified control points of the 1000 simulation runs is 3, whilst for epoch comparison epoch 1 vs. epoch 2_{10} one control point is most often identified as significantly deformed. Furthermore, the mean test value $\hat{F}$ for all epoch comparisons are smaller than those determined based on the refined models L = 1 and L = 2 (see Table 1 and 3), indicating lower statistical power.

ep.	Congruency Test		Localization
1 vs.	mean($\hat{F}$) (σ)	F($\alpha = 5\%$)	mode(sig. CP)
$\mathbf{2_0}$	0.999 (0.117)	1.200	0 of 49
$\mathbf{2_{10}}$	1.684 (0.177)		1 of 49
$\mathbf{2_{20}}$	3.099 (0.366)		3 of 49

Table 2. Comparison of results of the congruency test and localisation for the epoch comparisons based on surface representation L = 0 over all simulation runs

In Figure 7, a result of the deformation analysis for one representative realisation of the simulation runs is visualized. In comparison to the previous results in Section 4.1, one aspect can be recognized directly: A coarser TP B-spline surface resolution relative to the nominal ones results in a larger influence region for significantly deformed control points. Concerning the magnitude of determined deformation among significantly detected CP, the present interepochal Euclidean distance shown in Figure 7 is 5mm with a standard deviation of 0.6mm. Thus, it deviates from the nominal difference by 50%. Out of all realisations of the simulation runs resulting in the most frequent outcome w.r.t. the number and identification of this control point, a mean Euclidean distance of 4.4mm is derived with a precision of repeated outcomes of 0.6mm. This corresponds to 56% from the nominal difference. The maximum surface distance of the realisation shown in Figure 7 amounts to 2.6mm with a standard deviation of 1.1mm. This aligns with the mean maximum distance over repeated outcomes over all simulation runs and corresponds to a deviation from the nominal surface deviation of 5.6mm by 54%.

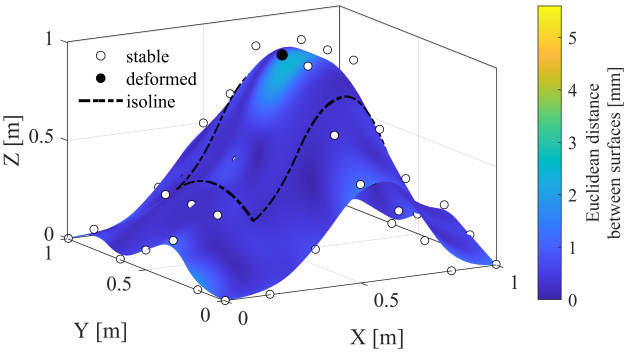

Figure 7. Representative result of the deformation analysis between epoch 1 and epoch 2_{10} based on surface representation L = 0

4.3 Deformation analysis based on surface representations of a higher refinement level

This section depicts the results of the deformation analyses when an additional level of refinement is added to the nested hierarchical B-splines. The added refinement level L = 2 is allocated in the region where initially deformation is simulated. The refined knot-grid is visualized in Figure 3(c).

This contribution has been peer-reviewed. The double-blind peer-review was conducted on the basis of the full paper.
https://doi.org/10.5194/isprs-annals-XI-1-2026-401-2026 | © Author(s) 2026. CC BY 4.0 License.

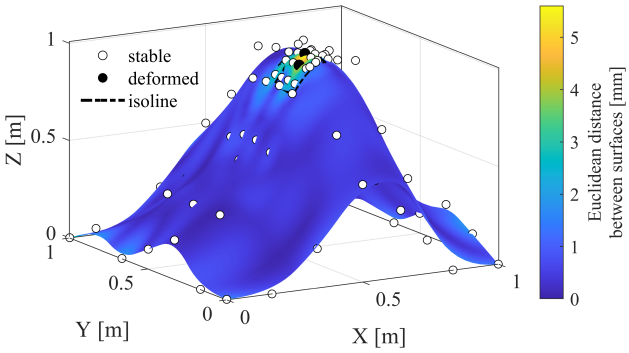

Figure 8. Representative result of the deformation analysis between epoch 1 and epoch 2_{10} based on surface representation L = 2

ep.	Congruency Test		Localization
1 vs.	mean($\hat{F}$) (σ)	F($\alpha = 5\%$)	mode(sig. CP)
$\mathbf{2_0}$	1.002 (0.093)	1.157	0 of 79
$\mathbf{2_{10}}$	1.758 (0.143)		2 of 79
$\mathbf{2_{20}}$	4.058 (0.239)		6 of 79

Table 3. Comparison of results of the congruency test and localisation for the epoch comparisons based on surface representation L = 2 over all simulation runs

The approximation of the point cloud from the reference as well as the respective comparison epochs is conducted with no necessity to adapt the stochastic model in the GMM. The summary of results of the successive deformation analysis based on the estimated control points over all simulation runs are stated in Table 3. For the epoch comparison epoch 1 vs. epoch 2_0 the null hypothesis applies likewise to the previous cases. In the other two epoch comparisons significant deformation is detected. Compared to the epoch comparison based on the nominal surfaces, a higher number of control points is significant. This is expected as the region covering present deformation is represented by comparably more control points.

For the representative realisation shown in Figure 8, the maximum deformation detected between significant control points is 8.5mm with a standard deviation of 2.2mm. This deviates from the nominal control point difference by 15%. The maximum distance between the surfaces of this realisation is 5.8mm with a standard deviation of 1mm, corresponding to an excess by 2% w.r.t. the nominal surface difference. Over all outcomes of the simulation runs that resolve to this - most frequent - number and identification of significant control points, the mean maximum distance of control points amounts to 8.5mm (15% deviation from nominal) accompanied by the precision of repeated outcomes of 1.7mm. The mean value of maximum surface distances of most frequent outcomes is 6.2mm (4% deviation from nominal) with a precision of repeated outcomes of 0.7mm.

4.4 Impact of neglection of partition of unity on the deformation analysis

At this point, it is important to specifically emphasize on the role of truncation. It ensures that the basis functions preserve their partition of unity throughout the nested structure of hierarchical B-splines (see Section 2.3). This characteristic is especially essential in the context of consecutive parameter-based deformation analysis as it requires invariance to affine transformation.

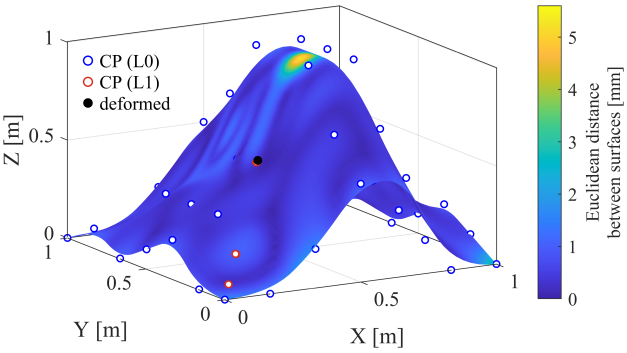

Figure 9. Results of the deformation analysis between epoch 1 and epoch 2_{10} based on a hierarchical B-spline surface representation without truncation of the B-spline basis

In Figure 9 the result of the deformation analysis based on the nominal surface representation is shown, where truncation was neglected in the respective surface approximations. Hereby, the basis functions become redundant and lead to unwanted influences in transition regions of different levels. The control points of the refined level are marked with red outlines and denoted as CP (L1). The estimated control points of L = 1 aggregate at three positions and thus overlap in the visualization. The absence of truncation impacts the estimation of their location. In the deformation analysis one control point is significantly deformed. It is marked as black point in Figure 9. Its location does not align with the region impacted by interepochal surface differences caused by the violation of partition of unity.

5. Discussion

Before analysing the results based on THBS surface, a strong emphasize is drawn on the importance of truncation in order to guarantee the preservation of partition of unity of the basis functions. This is essential for the stable estimation of control points in the GMM as well as for subsequently determining the correct deformation. In Section 4.4 the effect is demonstrated when truncation is neglected and the partition of unity characteristic is violated. The estimated control point loses its direct geometric association with the corresponding surface region, preventing its significance from being effectively propagated onto the surface. Consequently, the intended space-continuity of the deformation analysis is compromised.

If truncation is applied, the present results demonstrate the applicability of the congruence model on estimated control points for different levels of refinement.

The conducted deformation analyses based on THBS surfaces at three different levels of refinement, show notable differences in both the magnitude of identified deformations and the spatial extent of the significantly deformed regions.
The results show that the estimated magnitude of significant deformation is linked to the refinement of the surface representation. The coarser surface representations are, the less flexible the surfaces become. Consequently, local deviations in the point clouds may be underestimated when their spatial extent is smaller than the knot-grid spacing. The identified magnitudes of deformation based on both control point differences and surface differences derived in the simulation studies confirm this fact.

Moreover, the appropriate level of complexity of the B-spline surface is found if an additional step of refinement is added but the estimated deformation magnitude stays the same as that of the previous refinement level. This aspect can be seen by the consistency of magnitudes from the realisations based on the refinement levels L = 1 and L = 2.

Another notable insight can be derived from the standard deviations of the determined differences. In the present case, where the point clouds are superimposed by random, independent noise, the precision of the identified control point and surface differences decreases with increasing surface complexity. This is related to the number of points contributing to the estimation of the unknown control points. A surface of higher complexity contains more control points, each impacting a smaller area of the surface. Conversely, coarser B-splines surfaces have fewer control points, each linked to a larger area of the surface. If the variance covariance matrix of the point clouds is consistent across realisations, the differences of the number of contributing points causes variations in the precision of the estimations.

Regarding the spatial extent of the significantly deformed area, similar statements to the analysis of the magnitude can be drawn from the given results. The coarser the B-splines surface, the larger is the spatial extent of significantly deformed regions. In Figures 6, 7 and 8 the isolines indicate the regions of influence of the identified significant control points. This is mathematically related to the chosen degree of the surface. Certainly, these regions are also partly affected by neighboring non-significant control points. The relative influence of one control point on a specific surface point equals the corresponding weight derived from the basis functions (see Equation (1) and Equation (6)). This applies under the condition that the partition of unity of the basis functions is maintained.

Another observation can be drawn from the comparison of the number of significantly deformed control points determined in the epoch comparisons epoch 1 vs. epoch 2_{10} and epoch 1 vs. epoch 2_{20}: With an increase in deformation magnitude, more type-1 errors in the localization using surface models of inferior complexity w.r.t. the nominal result (see Table 2) arise. However, the usage of more complex surface models equally results in more control points being significant (see Table 3). This suggests that larger deformations exert a stronger influence on neighboring control points, thereby amplifying the detection of significant displacements.

While the present simulation study provides valuable insights into the effects of surface refinement, truncation, and the applicability of the congruence test, its limitations by the simplified noise model and idealized surface conditions shall be mentioned here. Real laser scans may include correlated noise, outliers, gaps, or highly localized deformations that could influence the estimation of control points and the detection of significant displacements. Despite these limitations, the results establish a solid foundation for the reliable application of THBS-based deformation analyses, and highlight areas for further investigation, such as testing under complex noise conditions and finer refinement sampling.

6. Conclusion

This paper comprises investigations in the context of space-continuous deformation analysis based on point clouds. The present approach is based on approximating B-spline surfaces. It features efficient data reduction due to a compact surface representation and allows for assessing deformations on the basis of estimated surface parameters, i.e. the control points. Spatial continuity of the deformation analysis is maintained as the control points are directly linked to distinct surface regions. The main contribution comprises the transition of the surface representation from global (TP) B-splines to THBS. Herethrough, the surface model and further the deformation detection and identification can be refined only in regions where needed. A strict condition for the applicability of the deformation analysis based on hiearchical surface representations comprises the truncation, being the modification of basis functions in overlapping regions of different refinement levels. Heretrough, the partition of unity is maintained and only then a trustworthy estimability of the control points is given.

Within a simulation environment, significant deformations between two point clouds were detected and identified by conducting the following pipeline: First the point clouds were each approximated using three nominal B-spline surface models of different refinement levels. Further, significant deformation was determined by introducing the respectively estimated control points in the congruency model. The present investigations are realised in a simulation environment and comprise three epoch comparisons based on surface representations with three different levels (L=0,1,2) of refinement. Synthetic point clouds generated by sampling nominal surface representations of L = 1 serve as observations. Results show that using B-spline representations of inferior complexity relative to the nominal surface (L = 0) may lead to type 1 errors in the deformation analysis and underestimation of deformation magnitudes. Contrary, B-spline surfaces of higher complexity (L = 2) show consistent deformation estimates w.r.t. both the determined deformation magnitude and the spatial extent of the significantly deformed surface region. This behaviour may serve as termination criterion for adaptive model refinement based on detected deformation.

Overall, the study demonstrates the applicability of THBS-based deformation analysis in a controlled simulation setting. Extending the approach to real-world laser scanning data represents a promising direction for future research.

Acknowledgements

This research was funded in whole or in part by the Austrian Science Fund (FWF) [10.55776/I6531]. Parts of the implementation of THBS are based on the Matlab package GeoPDEs 3.0 by Vázquez (2016).

References

Bureick, J., 2020. Robuste Approximation von Laserscan-Profilen mit B-Spline-Kurven. PhD thesis, Fachrichtung Geodäsie und Geoinformatik der Leibniz Universität Hannover.

Cox, M. G., 1972. The numerical evaluation of B-splines. *IMA Journal of Applied mathematics*, 10(2), 134–149.

D’Angella, D., Kollmannsberger, S., Rank, E., Reali, A., 2018. Multi-level Bézier extraction for hierarchical local refinement of Isogeometric Analysis. *Computer Methods in Applied Mechanics and Engineering*, 328, 147–174.

Dokken, T., Lyche, T., Pettersen, K. F., 2013. Polynomial splines over locally refined box-partitions. *Computer Aided Geometric Design*, 30(3), 331–356.

Dokken, T., Skytt, V., Barrowclough, O., 2015. Locally refined splines representation for geospatial big data. *The International Archives of the Photogrammetry, Remote Sensing and Spatial Information Sciences*, 40, 565–570.

Eichhorn, A., Heunecke, O., Kuhlmann, H., Neuner, H.-B., Welsch, W., 2013. *Auswertung geodätischer Überwachungsmessungen*. Wichmann eine Marke der VDE Verlag.

Forsey, D., Bartels, R., 1989. Local refinement editing of b-spline surfaces. *Proceedings on Graphics interface'88*, 125–126.

Garau, E. M., Vázquez, R., 2018. Algorithms for the implementation of adaptive isogeometric methods using hierarchical B-splines. *Applied Numerical Mathematics*, 123, 58–87.

Giannelli, C., Jüttler, B., Speleers, H., 2012. THB-splines: The truncated basis for hierarchical splines. *Computer Aided Geometric Design*, 29(7), 485–498.

Giannelli, C., Jüttler, B., Kleiss, S. K., Mantzaflaris, A., Simeon, B., Špeh, J., 2016. THB-splines: An effective mathematical technology for adaptive refinement in geometric design and isogeometric analysis. *Computer Methods in Applied Mechanics and Engineering*, 299, 337-365.

Harmening, C., 2020. Spatio-temporal deformation analysis using enhanced B-spline models of laser scanning point clouds. PhD thesis, Technische Universität Wien.

Hennig, P., Müller, S., Kästner, M., 2016. Bézier extraction and adaptive refinement of truncated hierarchical NURBS. *Computer Methods in Applied Mechanics and Engineering*, 305, 316-339.

Kerekes, G., 2023. An elementary error model for terrestrial laser scanning. PhD thesis, University of Stuttgart Germany.

Kermarrec, G., Hartmann, J., Faust, H., Hartmann, K., Besharat, R., Samuel, G., Lixian, C., Alkhatib, H., 2020. Understanding hierarchical B-splines with a case study: approximation of point clouds from TLS observations. *Z. Geodäsie Geoinf. Landmanagement*, 145, 224–235.

Kermarrec, G., Skytt, V., Dokken, T., 2022a. Locally refined b-splines. *Optimal Surface Fitting of Point Clouds Using Local Refinement: Application to GIS Data*, Springer, 13–21.

Kermarrec, G., Skytt, V., Dokken, T., 2022b. Surface approximation of coastal regions: LR B-spline for detection of deformation pattern. *ISPRS Annals of the Photogrammetry, Remote Sensing and Spatial Information Sciences*, 2, 119–126.

Kiss, G., Giannelli, C., Jüttler, B., 2014. Algorithms and data structures for truncated hierarchical b–splines. M. Floater, T. Lyche, M.-L. Mazure, K. Mørken, L. L. Schumaker (eds), *Mathematical Methods for Curves and Surfaces*, Springer Berlin Heidelberg, Berlin, Heidelberg, 304–323.

Mohammadivojdan, B., Lorenz, F., Artz, T., Weiß, R., Hake, F., Alkhatib, Y., Neumann, I., Alkhatib, H., 2025. Robust algorithm for automatic surface-based outlier detection in MBES point clouds. *Marine Geodesy*, 48(2), 141–172.

Mukupa, W., Roberts, G. W., Hancock, C. M., Al-Manasir, K., 2017. A review of the use of terrestrial laser scanning application for change detection and deformation monitoring of structures. *Survey review*, 49(353), 99–116.

Niemeier, W., 2008. *Ausgleichungsrechnung: Statistische Auswertemethoden*. Walter de Gruyter.

Ötsch, E., Harmening, C., Neuner, H., 2023. Investigation of space-continuous deformation from point clouds of structured surfaces. *Journal of Applied Geodesy*, 17(2), 151–160.

Ötsch, E., Neuner, H., 2025. Assessing approaches for consecutive b-spline model adaption based on point clouds with varying structural complexity. *9th International Conference on Engineering Surveying (INGEO))*, 10.

Pelzer, H., 1985. *Geodaetische Netze in Landes- und Ingenieurvermessung II: Vortraege des Kontaktstudiums Februar 1985 in Hannover*. Vermessungswesen bei Konrad Wittwer Band 13, Wittwer.

Piegl, L., Tiller, W., 2012. *The NURBS book*. Springer Science & Business Media.

Qin, R., Tian, J., Reinartz, P., 2016. 3D change detection – Approaches and applications. *ISPRS Journal of Photogrammetry and Remote Sensing*, 122, 41-56.

Raschhofer, J., Kerekes, G., Harmening, C., Neuner, H., Schwieger, V., 2021. Estimating control points for B-spline surfaces using fully populated synthetic variance–covariance matrices for TLS point clouds. *Remote Sensing*, 13(16), 3124.

Schwarz, G., 1978. Estimating the dimension of a model. *The annals of statistics*, 461–464.

Sederberg, T. W., Zheng, J., Bakenov, A., Nasri, A., 2003. T-splines and T-NURCCs. *ACM transactions on graphics (TOG)*, 22(3), 477–484.

Skytt, V., Barrowclough, O., Dokken, T., 2015. Locally refined spline surfaces for representation of terrain data. *Computers & Graphics*, 49, 58–68.

Vázquez, R., 2016. A new design for the implementation of isogeometric analysis in Octave and Matlab: GeoPDEs 3.0. *Computers Mathematics with Applications*, 72(3), 523-554.

Winiwarter, L., Esmorís Pena, A. M., Weiser, H., Anders, K., Martínez Sánchez, J., Searle, M., Höfle, B., 2022. Virtual laser scanning with HELIOS++: A novel take on ray tracing-based simulation of topographic full-waveform 3D laser scanning. *Remote Sensing of Environment*, 269, 112772.

This contribution has been peer-reviewed. The double-blind peer-review was conducted on the basis of the full paper.
https://doi.org/10.5194/isprs-annals-XI-1-2026-401-2026 | © Author(s) 2026. CC BY 4.0 License.